Energy balance, efficiency and operational limits of the dynamo type flux pump

Energy balance, efficiency and operational limits of the dynamo type flux pump

A. Morandi, G. Russo, M. Fabbri, L. Soldati

University of Bologna, Department of Electrical, Electronic and Information Engineering, 40136 Bologna, Italy

Abstract: In rotating flux pumps a rectified voltage, with non-zero DC component, is obtained at the terminals due to the combined effect of the distributed AC electromotive force, produced by one or more permanent magnets in circular motion, and the non-linear resistivity of the superconductor. Overcritical currents are continuously induced in the tape during operation, giving rise to the DC voltage and producing, at the same time, dissipation. In this paper the energy behavior of the flux pump is numerically investigated. It is shown that induced currents interact with the rotating magnet(s), producing a resistant torque that is little affected by the output current of the flux pump. Due to this interaction mechanism, a significant part of the mechanical power supplied to the rotor is converted into Joule heating within the tape. The paper also explores the operational limits of the flux pump, showing that the generator operation, involving an electric power delivered to the load combined with a mechanical power supplied to the rotor, can only be achieved in a restricted range of current and voltage at the terminals and that the maximum power transfer and efficiency are reached at the middle of the generator range. In no conditions the mechanical torque produced on the rotor can be reversed, reaching the motor mode involving an electric power absorbed at the terminals combined with a mechanical power produced on the rotor. A revised equivalent circuit comprising, besides the effective resistance reported in the literature, a further intrinsic resistance is proposed in the paper for taking all the dissipation mechanisms into account. It is shown that this equivalent circuit can predict the energization of an RL load both concerning the final steady values and the full time-domain behavior of the current (including ripples).

Keywords: HTS dynamo, flux pump, equivalent circuit, fem modelling, HTS tape.

I. INTRODUCTION

Compared to LTS, HTS magnets suffer greater magnetic field decay when operating in persistent current mode due to the low n-value and the higher joint resistance. In order to maintain a persistent current in HTS coils, connection to an external power supply at ambient temperature is required which, until now, has been achieved through the use of currents leads. The currents leads, however, can be bulky and long, thus expensive. Moreover, they greatly increase the overall thermal load of the system thus reducing the efficiency. Furthermore, when used for rotating machines, they require the use of brushes and slip rings, which can be extremely challenging to build and ultimately reduce the reliability and efficiency of the whole system.

A low-cost and compact alternative to the use of current leads is represented by flux pumping. Since the extensive survey provided by van der Klundert and ten Kate was published [1]-[2], different flux pumps concepts have been proposed [3]-[11]. An updated perspective of flux pumps topologies and operation can be found in [13]-[14]. Although the physical mechanism of flux pumps has been under debate, several experimental tests have shown their ability to inject large currents into HTS coils without the need for direct electrical connection [8]-[9]. Flux pumps could therefore lead to a tipping point in superconducting magnet implementation, provided that the assessment of loss performance is fully worked out and viability of full-scale systems for practical application is proved.

Exploring flux pumps behavior through accurate numerical models represents a fast and efficient method to provide optimal design criteria and to explore their losses and possible limits during practical operation. Several numerical models have now demonstrated the possibility to accurately reproduce the behavior of a dynamo type flux pump in no load condition [15]-[20], predicting the onset of the DC output voltage across the terminals in agreement with experimental measurements. More recently, numerical models able to simulate the dynamo type flux pump connected to a load (a DC current source or a coil) have been introduced [21], and successfully validated against experimental results [22]. Since the flux pump's main purpose is the energization of HTS magnets, the ability to predict the charging dynamic and the steady state coil's current, as well as the current ripple, is the mandatory step for the design of flux pump device of interest in practical applications. Of utmost importance is also the identification and the quantitative assessment of loss phenomena during operation and the identification of possible current and voltage limits that the flux pump could not overcome. In this paper, the energy behavior and efficiency of the flux pump are numerically investigated. The operational limits, experimentally confirmed in [23], beyond which the device cannot operate as a generator, delivering electric power to the load and absorbing mechanical power on the rotor, are also investigated. A revised empirical equivalent circuit, able to properly take all dissipation mechanisms into account, is also proposed and used for reproducing the energization of an RL load both concerning the final steady values and the full time-domain behavior of the current

(including ripples). This new equivalent circuit integrates the existing one, widely used for successfully reproducing the load behaviour [4]-[8], [14]-[15], [18], [21], [24] by adding an intrinsic resistance that accounts for the dissipation (occurring also in no load condition) associated to induced currents responsible of the rectification effect.

This paper is divided as follows: in section II, the considered apparatus and operating conditions are described. In section III, the numerical model, based on the volume integrate equation method (VIE) [26]-[29], and the energy balance calculation are explained. In section IV all the results are reported and discussed. A serviceable equivalent circuit is also derived in section IV, showing that the same performances of the flux pumps in terms of losses and magnets energization can be obtained via this faster and more convenient approach. The conclusions of the study are summarized in section V. It must be pointed out that the purpose of this paper is developing pragmatic methodology and indicators for investigating the most practical aspects and performance of flux pump, such as the efficiency, the power output and the operational limits in terms of voltage and current. Hence, as a first step, a constant critical current density J_c, independent of the magnetic field B, is considered throughout this work as in [16], [21]. It is pointed out, however, that the dependence of J_c on B may significantly improve the performance of the flux pump [15], [17], [20], [22], [30] though leaving the general trends and findings of the paper unchanged. The quantitative assessment of the impact of this dependence on the performance of the flux pump will be the subject of future work.

II. THE SIMULATED APPARATUS AND OPERATING CONDITIONS

The dynamo flux pump reported in [15], [16], [21] is considered in this work. The device consists of a 12 mm width HTS wire exposed to the field produced by a permanent magnet rotating anticlockwise past the wire with angular velocity ω. An external two-terminal component (or load) can be connected to the terminals of the HTS wire, and the overall behavior of the system is affected by the type of component. A 3D view of the flux pump connected to the external component is shown in Figure 1.a, where the current I and the voltage V denote the total delivered current and the voltage appearing at the terminal of the flux pump respectively. The *generator convention*, whereby the reference direction of the voltage is oriented toward the outgoing terminal of the current, is assumed for the flux pump. With this assumption a positive VI product denotes a power supplied by the flux pump and absorbed by the external component, and vice versa. Both the current I and the voltage V can, in general, change with time. Two different operating conditions will be considered for the flux pump in the following:

1. *Current driven operation* – the flux pump is connected to an external ideal current source that imposes the delivered current I. The open circuit operation of the flux pump can be seen as a limit case of this operating condition in which $I = 0$.
2. *RL load* – the flux pump is connected to an HTS coil. Electrically, this is equivalent to an external RL load where with resistance R_{ext} and inductance L_{ext} accounting for the joints and the superconducting winding respectively. This operating condition can be used to model the charging of a HTS coil up to any current below the critical value. The short circuit operation of the flux pump can be seen as the limit case in which $R_{ext} = 0$ and $L_{ext} = 0$, though this operating condition has no practical interest. In this work we consider a superconducting coil with 0.24 mH inductance and 0.88 μΩ resistance due to joints, as in [21]. Besides the joints, no further resistive effects are considered for the HTS coil.

We report that different operating conditions, possibly including voltage sources, could be modelled depending on the final application of the flux pump, but these are out of the scope of this paper and will not be considered. A schematic 2D section view of the flux pump is shown in Figure 1.b. All the relevant parameters of the considered flux pump are summarized in Table 1. A critical current of 283 A is assumed for the HTS wire. As discussed, no dependence of the critical current on the magnetic field is assumed. If needed this dependence can be integrated into the numerical model of section III with no substantial impact on the general conclusion arrived at in the rest of the paper.

Table 1 HTS dynamo parameters [15], [16], [21]

Width of the PM, a^{PM}	6 mm
Height of the PM, b^{PM}	12 mm
Depth of the PM, l^{PM}	12.7 mm
Remanence of the PM, B_r	1.25 T
Width of the HTS tape, a^{tape}	12 mm
Thickness of the HTS layer, b^{HTS}	1 μm
Critical current (77K, self field), I_c	283 A
n value	20
External radius of the rotor, R^{rotor}	35 mm
Airgap between the PM and the HTS tape, δ	3.7 mm
Frequency of rotation of the PM, f	25 Hz (1500 rpm)
Angular velocity of the PM, ω	157.08 rad/s

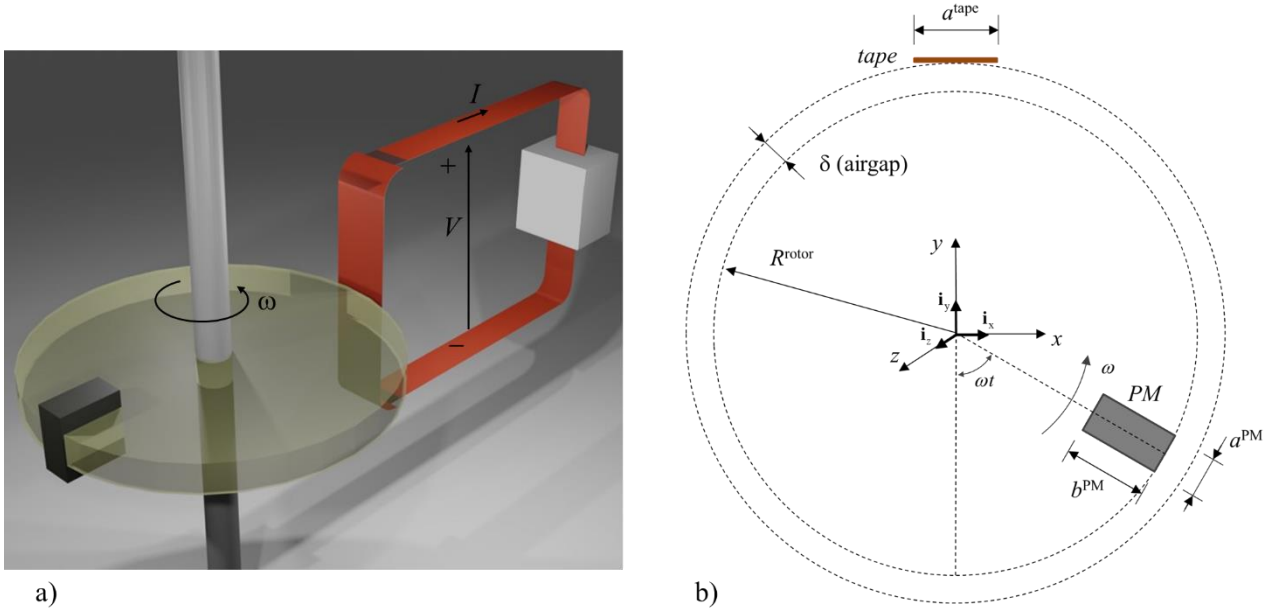

Figure 1 a) 3D view of the flux pump connected to the external component. B) schematic 2D section view of the flux pump (adapted from [16])

III. THE MODEL AND THE ENERGY BALANCE OF THE FLUX PUMP CONNECTED TO THE EXTERNAL COMPONENT

The numerical model used in this study is an extension of the VIE-based equivalent circuit previously used and briefly explained in [16]. In particular, the model has been expanded in order to simulate the operating conditions described in section II (whereas only no load operation could be dealt with in [16]). The details of the model are described in this section.

In the considered system the total electromotive force is given by the sum of a transformer-like contribution due to the time-varying field produced by the current induced in the superconductor and a second contribution due to the movement of the PM. As a consequence, the Faraday's law at any point in the superconductor gives [25]

$$\mathbf{E} = -\frac{\partial \mathbf{A}^{\mathrm{J}}}{\partial t} - \mathbf{v} \times \mathbf{B}^{\mathrm{PM}} - \nabla \varphi \tag{1}$$

where $\mathbf{A}^{\mathrm{J}}$ is the vector potential of the currents of the superconductor, $\mathbf{B}^{\mathrm{PM}}$ is the field of the permanent magnet, $\mathbf{v}$ is the velocity of $\mathbf{B}^{\mathrm{PM}}$ at the considered point and φ is the electric scalar potential. It is reported that term $-\mathbf{v} \times \mathbf{B}^{\mathrm{PM}}$ in equation (1) can be replaced by $-\partial \mathbf{A}^{\mathrm{PM}} / \partial t$, where $\mathbf{A}^{\mathrm{PM}}$ is the vector potential of the field of the permanent magnet, as in [17], [20], [21] . We assume the power

law as the constitutive equation relating the electric field **E** to the current density **J** of the superconductor, hence equation (1) is rewritten as follows

$$\rho(J)\mathbf{J} = -\frac{\partial \mathbf{A}^{\mathrm{J}}}{\partial t} - \mathbf{v}\times\mathbf{B}^{\mathrm{PM}} - \nabla\varphi$$
$$\text{with} \quad \rho(J) = \frac{E_0}{J_{\mathrm{c}}}\left(\frac{J}{J_{\mathrm{c}}}\right)^{n-1} \tag{2}$$

The dependence of the critical current J_c on the magnetic field could be taken into account. However, as it has been motivated in section I, in the following a constant critical current J_c is assumed since the general conclusions that are obtained in this paper are not affected by this dependence.

Based on equation (2) the numerical model of the flux pump can be obtained, after subdividing the conducting domain in a finite number of elements, by applying the volume integral equation method [26] In particular, a 3D model can be obtained by using the approach discussed in [27] for levitation problems. A 2D model can also be obtained under simplifying assumptions and is discussed in detail in the following. Both the 2D and 3D models take the form of an equivalent circuit that arises from strict FEM theory with no ad hoc assumptions. The constraints imposed by the external component coupled with the flux pump play the role of boundary conditions and are naturally included in the circuit model developed.

III.a The 2D FEM model of the flux pump

The cartesian reference frame (*x*, *y*, *z*) shown in Figure 1.b, with the *z*-axis parallel to the long dimension of the HTS wire, is introduced. We denote with $\mathbf{i}_{\mathrm{x}}$, $\mathbf{i}_{\mathrm{y}}$ and $\mathbf{i}_{\mathrm{z}}$ the unit vectors of the reference frame. For obtaining the 2D model we use the infinite long approximation, that is, we assume that all along the wire length the induced current only flows in the z-direction, that the field produced by the PM only lies in the cross section of the wire (the *xy* plane) and that neither the field nor the current depend on the *z* coordinate. This corresponds in practice to neglecting the effects of the terminal sections (at the ends of the PM, or where the HTS tape is connected to the external component in case of PM longer than the tape) where both the current and/or the field of the PM can follow a more complex path. It is worth to note that since the induced current **J** only flows in the z-direction also the magnetic vector potential $\mathbf{A}^{\mathrm{J}}$ associated with it only has *z* component. The permanent magnet along with the flux lines of the produced magnetic field can be considered as a unique rigid body rotating with angular velocity ω around the center *O* of the flux pump. Thus, the velocity **v** of the field at the generic point $\mathbf{r} = x\mathbf{i}_{\mathrm{x}} + y\mathbf{i}_{\mathrm{y}}$ of the cross section is given by

$$\mathbf{v} = \omega\,\mathbf{i}_{\mathrm{z}} \times \mathbf{r} \tag{3}$$

By expressing the Faraday's law (2) for the infinite long case depicted above and by using equation (3) we obtain[1]

$$\rho(J)\,J = -\frac{\partial A^{\mathrm{J}}}{\partial t} - \omega\,\mathbf{r}\cdot\mathbf{B}^{\mathrm{PM}} - \nabla\varphi \tag{4}$$

It can be seen from equation (4) that only the radial component of the magnetic field produced by the PM contributes to generating the motional electromotive force exciting the system. The numerical solution of equation (4) is obtained by using the weighted residual approach, explained in detail in [28]. The superconductor cross section is subdivided into a finite number of rectangles. An element-wise uniform distribution of current is assumed, and it is required that equation (4) be satisfied in the weak form over each element of the discretization [28]-[29]. In essence, by means of this procedure, the whole conducting domain is subdivided in a number N of thin wires with rectangular sections, and the following solving system is obtained

$$\mathbf{M}\frac{d}{dt}\mathbf{I}_{\mathrm{w}} = -\mathbf{R}\,\mathbf{I}_{\mathrm{w}} - \mathbf{U} - \mathbf{1}\nabla\varphi \tag{5}$$

where $\mathbf{I}_{\mathrm{w}}$ is the set of currents of the thin wires, $\mathbf{1}$ is a column vector of as many ones as the number of thin wires of the subdivision, $\mathbf{M}$ is the matrix of self/mutual induction coefficients, $\mathbf{R}$ is the diagonal matrix of resistances, $\mathbf{U}$ is the vector of motional electromotive forces acting on the thin wires with unit length and are defined by[2]

$$\begin{aligned} m_{hk} &= \frac{\mu_0}{4\pi}\int_{S_h}\int_{S_k} \ln\frac{1}{\left|\mathbf{r}-\mathbf{r}'\right|^2}\,dS'\,dS \\ r_{hh} &= \rho\left(\frac{I_h}{S_h}\right)\frac{1}{S_h}, \quad r_{hh} = 0 \quad \text{if} \quad h \neq k \\ u_h &= -\omega\frac{1}{S_h}\int_{S_h}\mathbf{r}\cdot\mathbf{B}^{\mathrm{PM}}\,dS \end{aligned} \tag{6}$$

By multiplying equation (5) for the active length of the flux pump, that is the depth l^{PM} of the permanent magnet, the following equation is finally obtained

---

[1] For obtaining the expression of the motional electromotive force term in equation (4) we have used $\mathbf{v}\times\mathbf{B}^{\mathrm{PM}} = (\omega\mathbf{i}_z\times\mathbf{r})\times\mathbf{B}^{\mathrm{PM}} = -\omega(\mathbf{i}_z\cdot\mathbf{B}^{\mathrm{PM}})\mathbf{r} + \omega(\mathbf{r}\cdot\mathbf{B}^{\mathrm{PM}})\mathbf{i}_z = \omega(\mathbf{r}\cdot\mathbf{B}^{\mathrm{PM}})\mathbf{i}_z$

[2] We report that the value at the center can be considered instead of the average on the h-th element for defining coefficients m_{hk}, r_{hh} and u_{h} in equation (6). Such an approach, consisting of assuming as weighting function the Dirac delta function $\delta(\mathbf{r}_{\mathrm{h}})$ at the center of the elements instead of the element wise unform weighting function $1/S_{\mathrm{h}}$, do not produce significant difference in the results.

(7) $$l^{PM}\,\mathbf{M}\frac{d}{dt}\mathbf{I}_{\mathrm{w}} = -l^{PM}\,\mathbf{R}\,\mathbf{I}_{\mathrm{w}} + l^{PM}\,\mathbf{U} - \mathbf{1}V$$

Where V is the voltage across the flux pump (see Figure 1.a) given by

(8) $$V = l^{PM}\ \nabla\varphi$$

The total current I circulating in the flux pump (see Figure 1.a), and in the external component connected to it, is given by the sum of currents of the wires and can be formally expressed as

(9) $$I = \mathbf{1}^{\mathrm{t}}\ \mathbf{I}_{\mathrm{w}}$$

Equations (7) and (9) correspond to the finite element based equivalent circuit of Figure 2.a and Figure 2.b, referring to the flux pump operating in current driven mode (i.e., connected to a current source) or supplying a RL load respectively. This equivalent circuit of the flux pump contains, per each branch, a voltage source u representing the electromotive force impressed by the moving magnet, a non-linear resistor r, accounting for the resistive voltage drop inside the superconductor, and a coupled inductor representing the electromotive force induced by the time-varying field produced by the current of the superconductor. All the branches are connected to the external component (current source or RL load, in the cases considered here) carrying the total current I and subject to the voltage V of the flux pump. In order to solve the problem, the constitutive equation of the external component needs to be specified. If the flux pump is connected to an ideal current source, then the total current is an assigned quantity and equations (7) and (9) form an algebraic-differential system that can be solved yielding, at any instant, the current distribution within the flux pump (vector $\mathbf{I}_{\mathrm{w}}$) and the voltage V across it. Once the voltage V is calculated at any instant, the average value in one period $T=2\pi/\omega$ of rotation can be defined as

(10) $$V_{average} = \frac{1}{T}\int_{t}^{t+T} V(t')\,dt'$$

On the other hand, if the flux pump is connected to an RL load, then the voltage V across it is subject to

(11) $$V = R_{ext}\,I + L_{ext}\,\frac{d}{dt}I$$

Hence, by substituting (11) in (7) and by using (9), the following differential equation is obtained which allows to calculate the current distribution (vector $\mathbf{I}_{\mathrm{w}}$) at any instant.

(12) $$\left(l^{PM}\,\mathbf{M} + L_{ext}\mathbf{1}^{\mathrm{t}}\mathbf{1}\right)\frac{d}{dt}\mathbf{I} = -\left(l^{PM}\,\mathbf{R} + R_{ext}\mathbf{1}^{\mathrm{t}}\mathbf{1}\right)\mathbf{I} + l^{PM}\,\mathbf{U}$$

The voltage V of the flux pump can be obtained afterward by using equation (11), or one of the equations (7). The average voltage across the flux pump can finally be obtained by using (10).

It is stressed that, when operating with a current, either impressed by a current source or supplied to a coil, the flux pump is able to transfer power to the external component only if a non-zero and positive average voltage is generated across it.

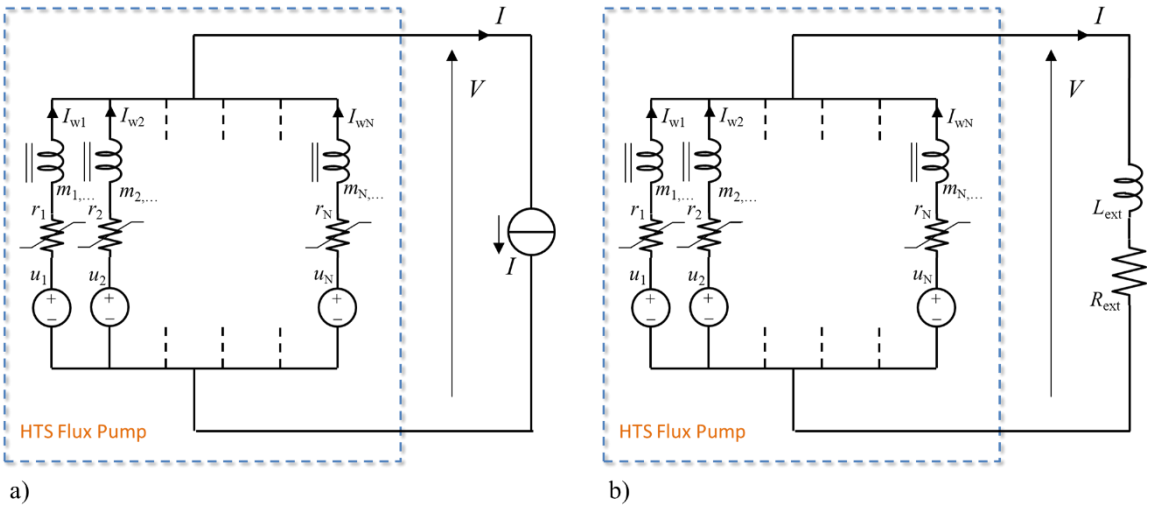

Figure 2. Finite element based equivalent circuit of the flux pump a) connected to a current source b) connected to an RL load

III.b. Energy balance and efficiency

For stating the energy balance, we start from the Faraday's law (4), that for the present purpose we rewrite in the following vector form

$$\rho J \mathbf{i}_z = -\frac{\partial A^J \mathbf{i}_z}{\partial t} - (\omega \mathbf{i}_z \times \mathbf{r}) \times \mathbf{B}^{PM} - \nabla \varphi \mathbf{i}_z \tag{13}$$

By taking the scalar multiplication of equation (4) by the vector current density $\mathbf{J} = J \mathbf{i}_z$ we obtain[3]

[3] For obtaining equation (12) we use $-(\omega \mathbf{i}_z \times \mathbf{r}) \times \mathbf{B}^{PM} \cdot J \mathbf{i}_z = J \mathbf{i}_z \times \mathbf{B}^{PM} \cdot \omega \mathbf{i}_z \times \mathbf{r} = -(J \mathbf{i}_z \times \mathbf{B}^{PM}) \times \mathbf{r} \cdot \omega \mathbf{i}_z$. Furthermore, as for the first term at the right-hand side, the scalar multiplication yields the term $-J \frac{\partial}{\partial t} A^J$. Due to the symmetry of the Green's function relating the magnetic vector potential to the current density we obtain $\frac{\partial}{\partial t}(J A^J) = J \frac{\partial}{\partial t} A^J + A^J \frac{\partial}{\partial t} J = 2J \frac{\partial}{\partial t} A^J$, which gives $J \frac{\partial}{\partial t} A^J = \frac{\partial}{\partial t}\left(\frac{1}{2} J A^J\right)$ as in (12).

(14) $$\rho J^2 = -\frac{\partial}{\partial t}\left(\frac{1}{2} J A^{\mathrm{J}}\right) - \left(J\,\mathbf{i}_{\mathrm{z}} \times \mathbf{B}^{\mathrm{PM}}\right) \times \mathbf{r} \cdot \omega \mathbf{i}_{\mathrm{z}} - J \nabla \varphi$$

By taking the integral of equation (14) over the volume occupied by the active length of the flux pump we obtain[4]

(15) $$-\omega l^{PM} \int_S \left(J\,\mathbf{i}_{\mathrm{z}} \times \mathbf{B}^{\mathrm{PM}}\right) \times \mathbf{r}\, dS = V I + l^{PM} \int_S \rho J^2 dS + l^{PM} \frac{\partial}{\partial t} \int_S \frac{1}{2} J A^{\mathrm{J}} dS$$

Which we finally rewrite as

(16) $$-T\omega = V I + P_{\mathrm{J}} + \frac{d}{dt} W_{\mathrm{mag}}$$

where P_{J} is the total joule loss occurring in the superconductor, W_{mag} is the stored magnetic energy and T is the resistant mechanical torque produced onto the rotor, via the Lorentz force, by the current of the superconductor and is given by

(17) $$T = l^{PM} \int_S \left(J\,\mathbf{i}_{\mathrm{z}} \times \mathbf{B}^{\mathrm{PM}}\right) \times \mathbf{r}\, dS$$

Equation (16) states that, at any instant, the mechanical power $P_{\mathrm{mechanical}} = -T\omega$ supplied to the rotor is transferred, up to the dissipation P_{joule} and the change dW_{mag}/dt of magnetic energy of the superconductor, to the external component connected to the flux pump whose absorbed power is given by

(18) $$P = V I$$

Since during cyclic operation no net change of the magnetic energy occurs, the net mechanical energy E_{m} supplied to the rotor in one cycle, is in part transferred through the terminals to the external component and in part dissipated into the superconductor due to Joule heating. Accordingly, by denoting with E and E_{joule} the transferred electrical energy and the dissipated energy respectively, the efficiency of the flux pump can be defined as

---

[4] The discrete equivalent of equation (15), based on the equivalent circuit model introduced in section III.a, is given by

(i) $$\omega l^{PM} \sum_h I_h \left(x_h B_{x,h}^{\mathrm{PM}} + y_h B_{y,h}^{\mathrm{PM}} \right) = V I + \sum_h \rho_h \frac{l^{PM}}{S} I_h^2 + \frac{d}{dt}\left(l^{PM} \frac{1}{2} \sum_h \sum_k m_{hk} I_h I_k \right)$$

where the four terms appearing represent the calculated mechanical power of the rotor, the power transferred to the load, the total joule loss and the change of magnetic energy of the superconductor, respectively, and the sums involve all the elements of the discretization.

(19) $$\eta = \frac{E}{E_{\text{mechanical}}} = \frac{E}{E + E_{\text{joule}}} = \frac{\int_{t}^{t+T} VI\, dt'}{-\int_{t}^{t+T} \omega T\, dt'}$$

IV. NUMERICAL RESULTS, DISCUSSION AND EMPIRICAL EQUIVALENT CIRCUITS OF THE FLUX PUMP

The results obtained by means of the model of section III are shown and discussed in this section and the operational limits of the flux pump are investigated. All results shown were obtained by including in the model the superconductor layer only [16]-[21] and neglecting the other constituents of the composite HTS tape, namely the substrate and the shunt layer. The inclusion of these further layers in the model implies a higher number of variables and a longer calculation time and does not change significantly the conclusion arrived at in this section. Furthermore, the results shown were obtained by meshing the HTS layer with 60 elements, obtained by using 60 subdivisions along the tape width and 1 subdivision along the layer's thickness. The use of only one subdivision along the thickness is equivalent to assuming the thin sheet approximation for the superconductor's current [31]. More subdivisions can be used for modeling the distribution of the current along the layer's thickness into account. We have verified, however, that no substantial difference emerges in the numerical results by using more subdivisions both along the width and the thickness of the tape.

The average motional electromotive force produced by the PM onto the elements (thin wires) of the discretization during one rotation cycle is shown in Figure 3. This is the voltage impressed by the voltage sources of the FEM-based equivalent circuit of Figure 2, corresponding to terms u_h in equations (6). They apply both for the current driven operation (Figure 2.a) and for the RL load (Figure 2.b). The curves shown in Figure 3 refer to elements of the subdivision lying at various positions along the tape's length. All electromotive forces have, individually, zero average value during one period. Nevertheless, it is their presence that, combined with the non-linearity of the superconductor, produce an average DC voltage at the terminal of the flux pump [20]. The highest electromotive force is obtained at the middle of the tape, which reaches up to 15.1 mV (absolute value), since this is the element closest to the PM (reaching the lower distance corresponding to the airgap δ of 3.7 mm – see Figure 1.b). Electromotive forces referring to symmetric positions during the rotation (e.g., begin and end of the tape, or ¼ and ¾ of the tape's width) have the same (mirrored) waveform but are displaced by the time needed by the PM to span the angle between them. In the case of tape bent along the circumference so to form an air gap constant in all positions the emf of all elements would have the same waveform, displaced in time. The minimum and the maximum emf occurring in the tape at any instant during the PM motion are also highlighted in Figure 3.

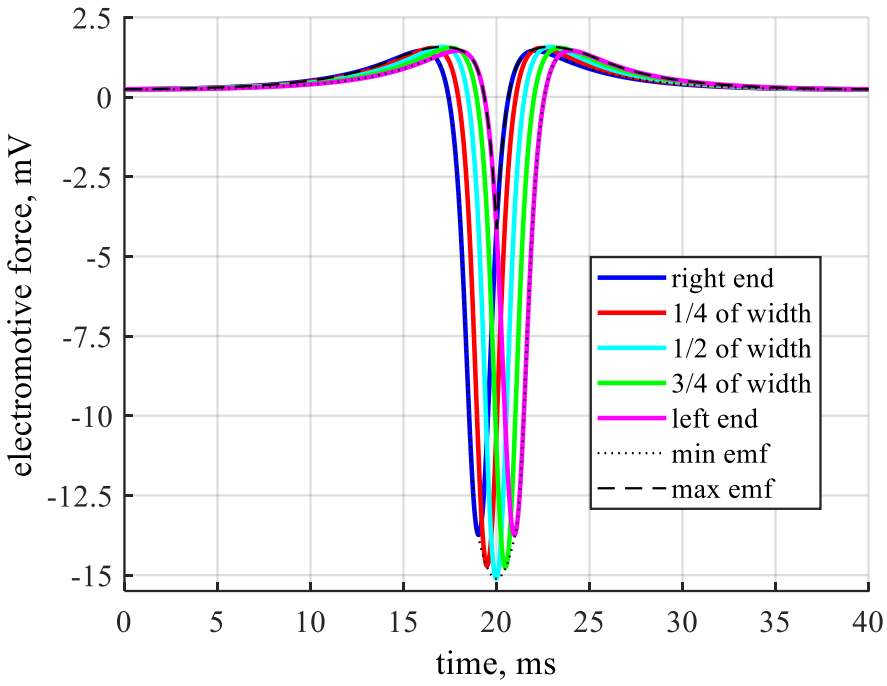

Figure 3. Electromotive force induced by the PM during one rotation cycle at various position along the tape's width a^{tape} (see Figure 1.b). The curves shown refer to the right end of the tape, ¼ of the width from the right, ½ of the width, at ¾ of the width from the right and to the left end of the tape. The minimum and the maximum emf occurring in the tape at any instant are also shown by means of dotted and dashed lines respectively.

IV.1 Current driven operation – terminals voltage, energy balance and simplified equivalent circuit

IV.1.a Terminal voltage

The behavior of the flux pump when it is connected to an ideal source impressing a DC current I is discussed in this section. The open circuit operation of the flux pump can be seen as the particular case in which $I = 0$. Results shown refer to the case where first the transport current is applied and after the rotation is started, and more in particular

- The impressed current is linearly increased from zero to its final DC value I during a time interval corresponding to two rotation periods. No rotation of the PM occurs during the ramp-up of the current.
- A resting interval, lasting one period of rotation, is applied after reaching the final value I. No rotation of the PM occurs during this interval.

- The PM starts to rotate after the resting interval while the impressed current is kept constant to the final value *I*. Cyclic operation of the flux pump is reached.

The terminal voltage *V* of the flux pump during one cycle is displayed in Figure 4 for various values of the current *I* impressed by the external source in the range from –20 A to +50A. The open circuit voltage of the flux pump, corresponding to *I*=0, is included in the figure. The maximum and minimum electromotive force acting all over the tape width during the cycle, taken from Figure 3, are also replicated in Figure 4. It can be seen that, for all impressed currents in the considered range, the terminal voltage is always comprised between the minimum and the maximum emf produced by the PM motion onto the tape. Moreover, despite the fact that all electromotive forces produced by the PM on the tape have zero average value (see Figure 3), the terminals' voltages of Figure 4 have non-zero average value in one cycle. This average can be positive or negative depending on the impressed DC current. To show this, the time integral of the terminal voltage during one cycle is shown in Figure 5, for the different impressed currents. The corresponding average voltage V_{average} of the flux pump in one cycle, obtained by means of equation (10), is shown in Figure 6 as a function of the impressed DC current *I*. It is clear from these figures that, besides the fluctuating time behavior of Figure 4, the terminals' voltage of the flux pump is characterized by a non-zero DC average when it operates with an impressed DC current in the considered range. This DC voltage component is the result of the distributed electromotive force produced by the PM on the tape combined with the non-linear resistivity of the superconductor (the inductive terms have, in fact, a negligible effect on the formation of the terminal voltage, a result already found in [21]). It is important to point out that, according to [20], and consistently with the predictions of the FEM-based equivalent circuit model of Figure 2, screening currents reaching overcritical values are continuously induced in the tape for producing the rectification effect at the terminals. These currents circulate also in no load condition (open circuit operation with $I = 0$) and have a major impact on the energy balance of the flux pump. It must be pointed out that, even though the instantaneous terminal voltage reaches well beyond 10 mV (absolute value), the average (DC component) voltage only reaches a few tens of μV, as discussed in detail later. It is important to note, from Figure 6, that the average (DC) voltage of the flux pump decreases linearly with the impressed DC current and reaches 0 V at $I = I_0 = 34.2$ A. Beyond this value, a negative DC voltage appears at the terminal of the flux pump. Hence, as far as the DC impressed current is in the range $[0 – I_0]$, due to the fact that positive current and average voltage are observed at the terminals, and since the generator convention is assumed for the reference direction of *I* and *V* (see Figure 1.a), a positive average power $P_{average} = V_{average} I$ is delivered in one period by the flux

pump, that operates in generator mode. However, if the DC impressed current is increased beyond I_0, the average voltage at the terminals reverses, as it is experimentally confirmed in [23], and the average delivered power becomes negative, meaning that the power is absorbed by the flux pump. Hence, value I_0 fixes the limit beyond which the flux pump exits the generator mode and enters the dissipative mode. Similarly, if the impressed DC current is negative, the average terminal voltage remains positive and a negative average delivered power is obtained, meaning that the flux pump is operating in the dissipative mode. It is important to point out that the described phenomenology concerning the shift between the generator and the dissipative mode beyond a certain current limit is experimentally proved [23], and the numerical model used in this paper provides results in agreement with that evidence. It is stressed that, despite the fact that a null average voltage occurs at the terminals corresponding to it, current I_0 should not be interpreted as the short circuit current of the flux pump. In fact, as it is discussed in section IV.b, if a short circuit connection is created at the terminals, a current with a much higher average value than I_0 is obtained. Hence, I_0 can only be assumed as the limit of the generation ability of the flux pump.

The open circuit voltage, corresponding to the operation of the flux pump with no impressed DC current ($I = 0$), is denoted with V_0 in Figure 6 and is 58.9 μV. The flux pump can only operate in the generator mode if the operating point lies in the first quadrant of the I-V_{average} plane, with both positive current and voltage. This only occurs if the impressed current is in the range [0 - I_0] and the corresponding average voltage is in the range [V_0 - 0]. Beyond these limits, either the voltage or the current becomes negative. The operating point falls respectively in the second or the fourth quadrant of the I-V_{average} plane, and a dissipative behaviour occurs. To better emphasize how the rotation of the PM affects the energy behaviour of the flux pump, in Figure 7 the average terminal voltage is compared with the voltage that would occur across the tape in case of no rotation, over a wide range of DC impressed currents. It is clear from the figure that the effects of the rotation are:

- Shifting the *VI* curve into the first quadrant allowing power generation. This is effect is clearly visible in Figure 6, which is a magnification of Figure 7 around the origin. In case of no rotation, the *VI* curve only lies in the second and fourth quadrant corresponding to the dissipative operation. However, the current and voltage intervals in which generation is allowed are very narrow. In particular, the maximum current I_0 (34.2 A) for which power generation is possible is much lower than the critical current I_c of the tape (283 A – see Table I). Supplying power to a load requiring a current greater than I_0 is not possible by means of the flux pump. It is stressed that, for fixed air gap and angular velocity, I_0 is an intrinsic parameter of the flux pump and does not depend on the load connects to it. It is also reported that if the direction of rotation is reversed, both V_0 and I_0 are reversed, as confirmed in [23].

Hence, the whole *VI* curve is translated downward in the second, third and fourth quadrants. In this case the generator mode occurs in the third quadrant and can only be obtained if the impressed current is reversed too.

- Increasing the power to be supplied for impressing a DC current when the flux pump does not operate in the generation mode. In fact, in case of no rotation, appreciable voltage (developed according to the power-law characteristic of the material) and, hence, power dissipation, only occurs for impressed currents well beyond the critical value. On the opposite, loss free current cannot be impressed in the tape if rotation is in progress since substantial voltage is detected even at small current and power must be supplied for keeping the current circulating, which is converted in AC loss into the tape.

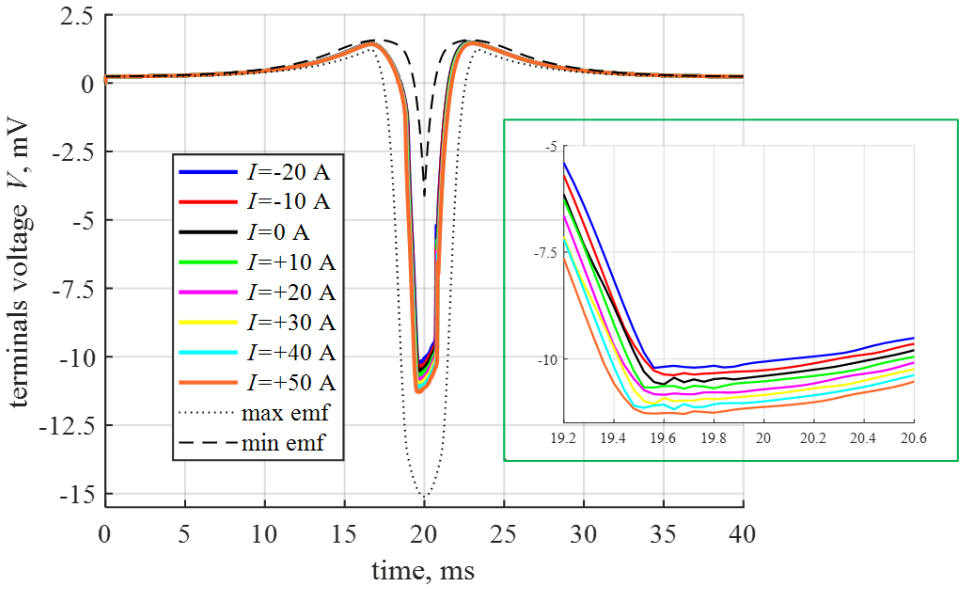

Figure 4. Terminal voltage *V* of the flux pump versus time in one cycle for various values of impressed DC current *I*. The black curve, corresponding to *I*=0, is the instantaneous open circuit voltage of the flux pump. The insert of the figure shows the detail of the waveform in a more restricted time interval. The monotone decrease of the terminal voltage with increasing current, visible in the insert, is observed at all instants of the cycle.

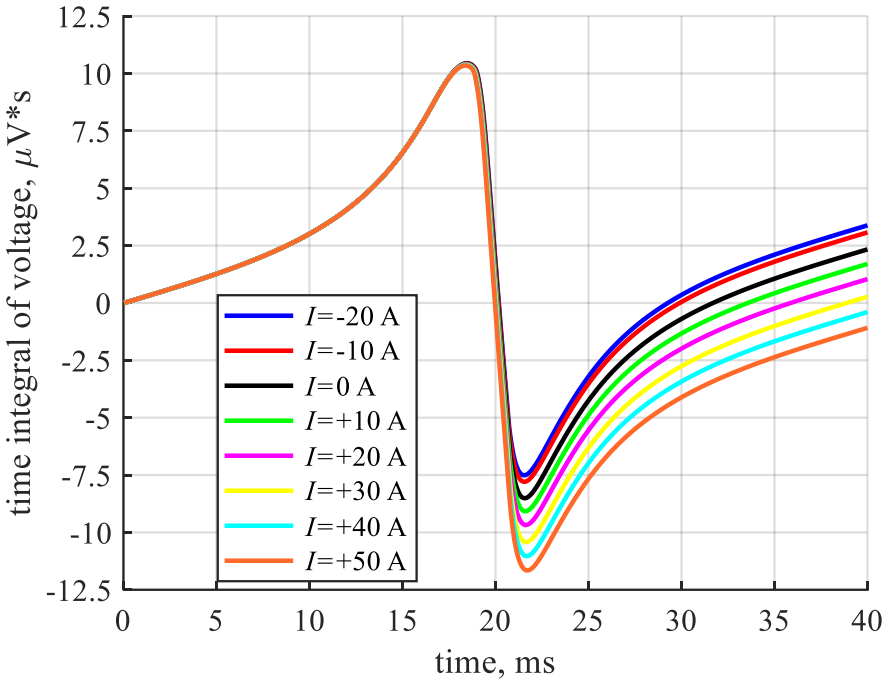

Figure 5. Time integral of the terminal voltage V of the flux pump during one cycle for various values of impressed DC current I.

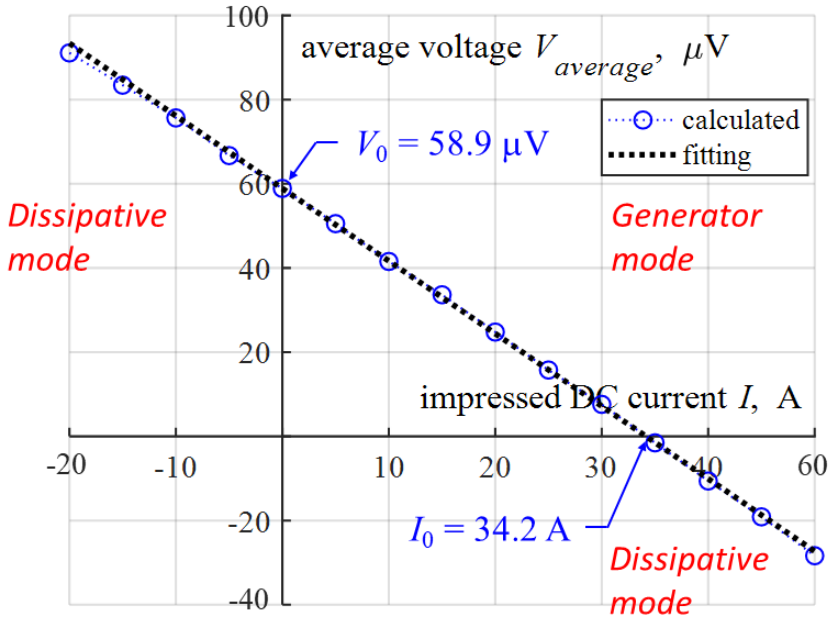

Figure 6. Average voltage $V_{average}$ of the flux pump in one cycle for various values of impressed DC current I. The dotted line represents the linear V-I trend intersecting the I and V axes at points (I_0, 0) and (0, V_0) respectively.

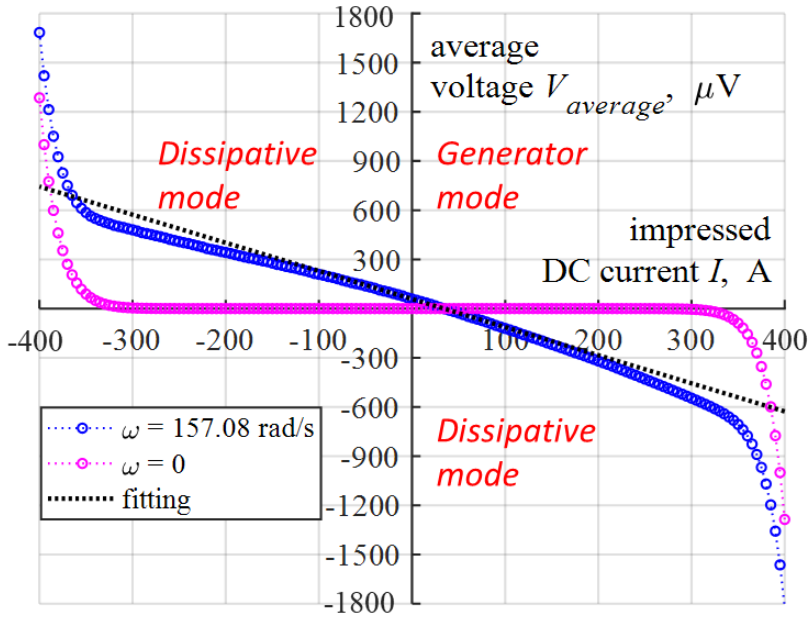

Figure 7. Average voltage $V_{average}$ of the flux pump rotating at 157.08 rad/sec (25 Hz) compared with the voltage developing at the tape's terminal in case of no rotation over a wide range of impressed DC currents. The dotted line represents the linear *V-I* trend intersecting the axes at points (I_0, 0) and (0, V_0) as in Figure 6.

IV.1.b Energy Balance

The discussion of the energy behaviour made in the previous paragraph *IV.1.b* only involved the power *P* exchanged with the external two-terminal component. For stating the overall energy balance of the flux pump further energy terms must be considered that are:

- the total joule heating P_{joule} produced, at any instant, within the tape
- the mechanical power $P_{mechanical}$ that must be supplied to the rotor for maintaining the rotation
- the change rate $P_{magnetic}$ of the magnetic energy stored in the magnetic field produced by the currents of the tape

The calculated time behaviour of the four power terms of the flux pump during one rotation period is shown in Figure 8 for different values of the DC impressed current. The corresponding energy during 10 cycles, obtained via the integration of the power terms, is shown in Figure 9. A monotone increasing trend can be observed in Figure 9 for the mechanical energy supplied to the rotor, for the energy dissipated into the tape due to Joule heating, and for the energy supplied by the external

component, meaning that net unidirectional energy transfer occurs. Mechanical energy is always positive meaning that no energy can be extracted from the rotor (motor behaviour). The net electric energy transferred to the external components can be both positive or negative, depending on if the flux pump operates in the generator or the dissipative mode respectively. In the latter case, the energy is indeed delivered by the external component to the flux pump and is converted, along with the energy supplied to the rotor, into heat into the tape. As expected, a cyclic behaviour is observed for the magnetic energy that, hence, does not contribute to the overall energy balance.

In the case of open circuit operation (I = 0 A) no power is exchanged at the terminals. Nevertheless, currents are induced in the tape during the rotation that generate the power loss P_{joule} and, at the same time, a non-zero average voltage at the terminals $V_{average} = V_0$ = 58.9 μV. This power is more intense when the magnet passes below the tape and reaches a peak of about 2.18 W. The dissipated energy in ten cycles is 54.38 mJ, corresponding to an average power of 135.9 mW. The induced currents create a resistant torque on the rotor, which requires mechanical energy to maintain the rotation. A total mechanical energy of 54.38 mJ is supplied to the rotor in ten cycles and is integrally converted in heat into the tape. When the flux pump operates with a DC impressed current I = 17.1 A (the half of I_0 – see Figure 6) it operates in the generator mode and transfers the maximum possible power to the load (the reason why the power is maximum in this condition is related to the linearity of the *V-I* curve in the first quadrant and is discussed in detail in paragraph *IV.1.c*). The instantaneous power exchange with the external component can be both positive and negative. Nevertheless, a positive average voltage $V_{average}$ = 30.1 μV is developed across the terminals, caused by the nonlinear *E-J* relation, which is responsible for the power transfer. The net energy transferred by the flux pump to the external load in ten cycles is 0.21 mJ, corresponding to an average power of 0.53 mW (also obtainable as $V_{average}$ I). The joule dissipation is 54.49 mJ. The mechanical energy transferred to the rotor in this operating condition is 54.70 mJ and is nearly completely converted in joule dissipation with only a small part (0.21 mJ) transferred to the load. When the DC impressed current is lower than zero or greater than the limit I_0 of the generator region (34.1 A) then the average voltage and power at the terminal of the flux pump reverse. Energy is transferred from the external component to the flux pump and is converted, along with the mechanical power supplied to the rotor, in dissipation into the tape. It is stressed that the joule heating is an inherent phenomenon, due to the overcritical currents induced by the rotation of the magnet in the tape [16],[20], and is little affected by the operating DC current of the flux pump. To show this, the profile of current density and the corresponding profile of power dissipation at the middle of the rotation cycle (t = 20 ms+kT) is shown in Figure 10. It can be seen that, as far as it does not overcome the critical value I_c, the impressed DC current I has a small effect on the current and power distribution within the tape, which are dominated by the rotation and

occurs also in case of no transport current. A minimum joule dissipation of 54.38 mJ is obtained in no load conditions, and the dissipation corresponding to different DC impressed currents, both in the generator mode and the dissipative mode, is only slightly higher. In all cases, the mechanical power supplied to the rotor equals the joule heating plus or minus the power exchanged with the external component, depending on if the flux pump operates in the generator or the dissipative mode respectively. Moreover, the power exchanged with the external component is much lower than the joule dissipation. As a result, the efficiency of the flux pump, calculated according to equation (19), is low. In case of maximum power transfer to the external load (0.52 mW at I = 17.1 A) an efficiency of 0.39 % is obtained. To further assess the energy performance of the flux pump, the average joule power, terminals' power and mechanical power in one cycle are shown in Figure 11a-c for different values of the DC impressed current. The corresponding efficiency is shown in Figure 11d. It is confirmed that:

- A positive average power is delivered to the external component by the flux pump, which acts as a generator, as far as the operating current is in the range [0 – I_0]. Outside of this interval the power is delivered by the external component and absorbed by the flux pump. In no case the mechanical power, supplied to the rotor, is negative (this is true over any current range, much wider than the one sown in Figure 11c). Hence, outside the generator mode, the flux pump only acts in the purely dissipative mode and never in the motor mode.
- Only a small part of the mechanical power supplied to the rotor is transferred to the external load in the generator region. This is due to the inherent dissipation associated with the induced current, responsible for the DC voltage, occurring also in no load conditions. As a result, the efficiency is low. A maxim efficiency of 0.39% is reached at 17.1 A (I_0 /2).

It must be reminded that a constant critical current density is being considered and that accounting for its dependence on the B field produces substantial improvement of the performance [15], [17], [20], [22], [30], reducing the Joule heating and increasing the efficiency. The quantitative assessment of this impact is beyond the scope of this paper and will be the objective of further studies.

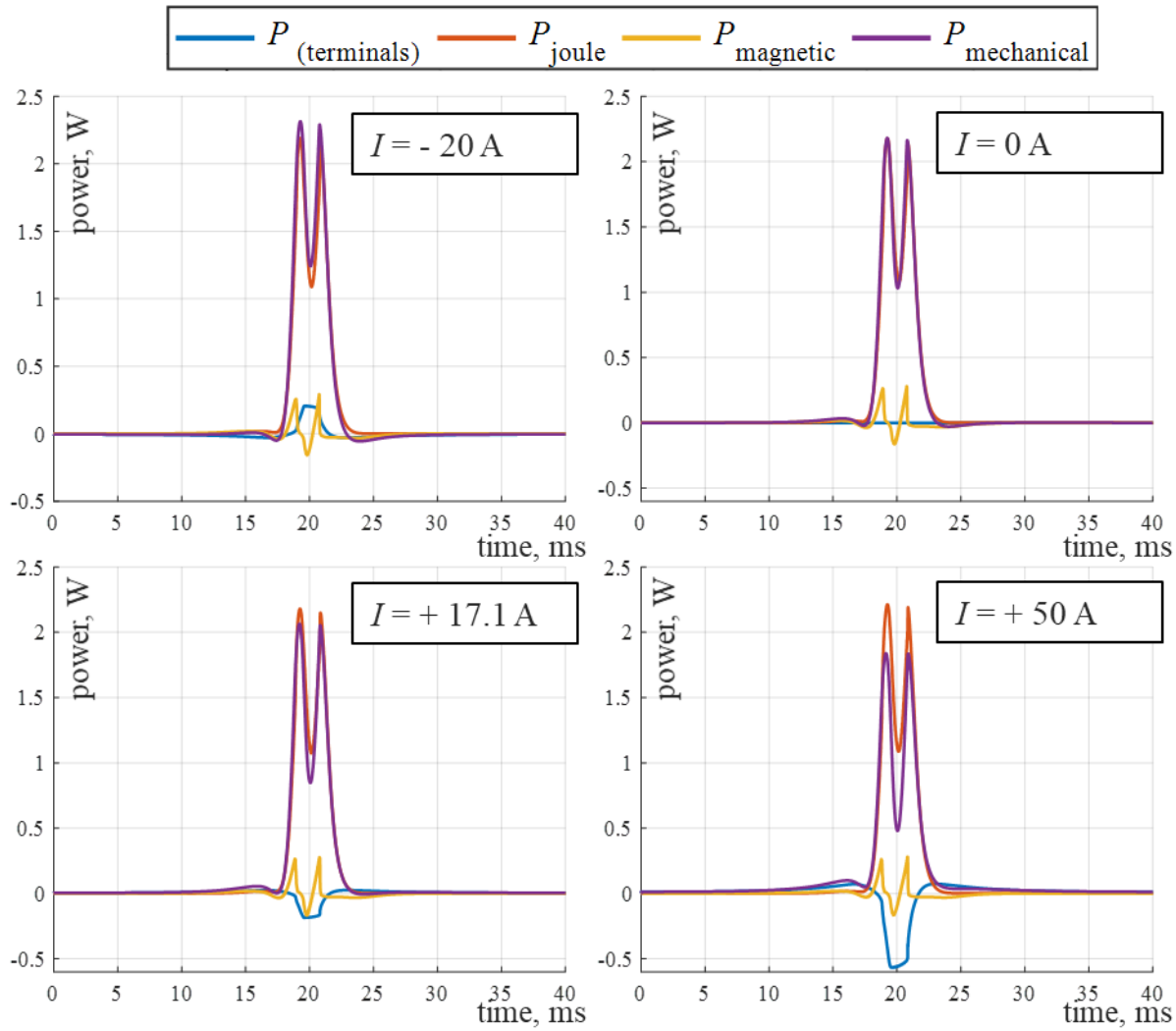

Figure 8. Power terms of the flux pump during one rotation cycle for different values of the DC impressed current.

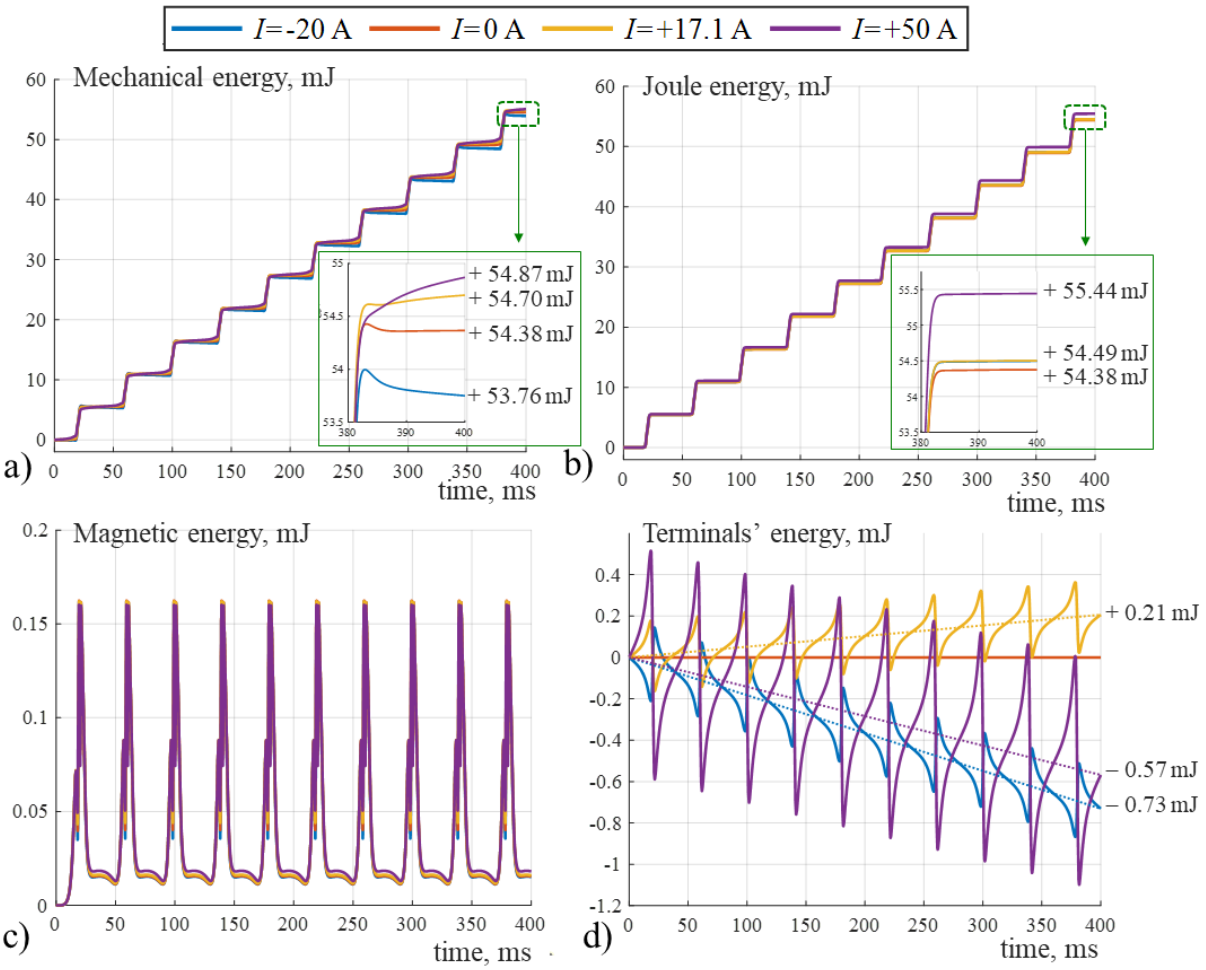

Figure 9. Energy terms of the flux pump during ten rotation cycles for different values of the DC impressed current. The dotted line corresponds to the energy exchanged by the flux pump with external load in case of operation with constant average power

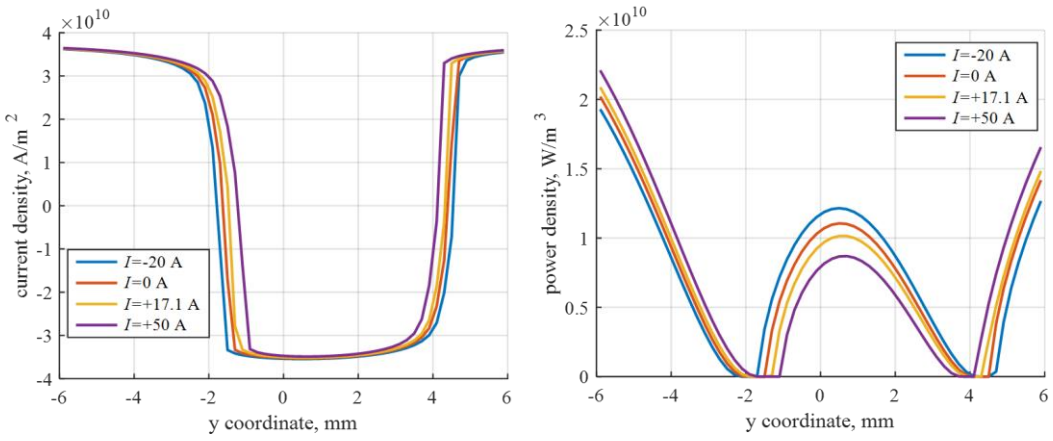

Figure 10. Profiles of current density and power density ($E \cdot J$) along the tape at t=20 ms (half cycle, magnet aligned with the tape) for different values of the DC impressed current.

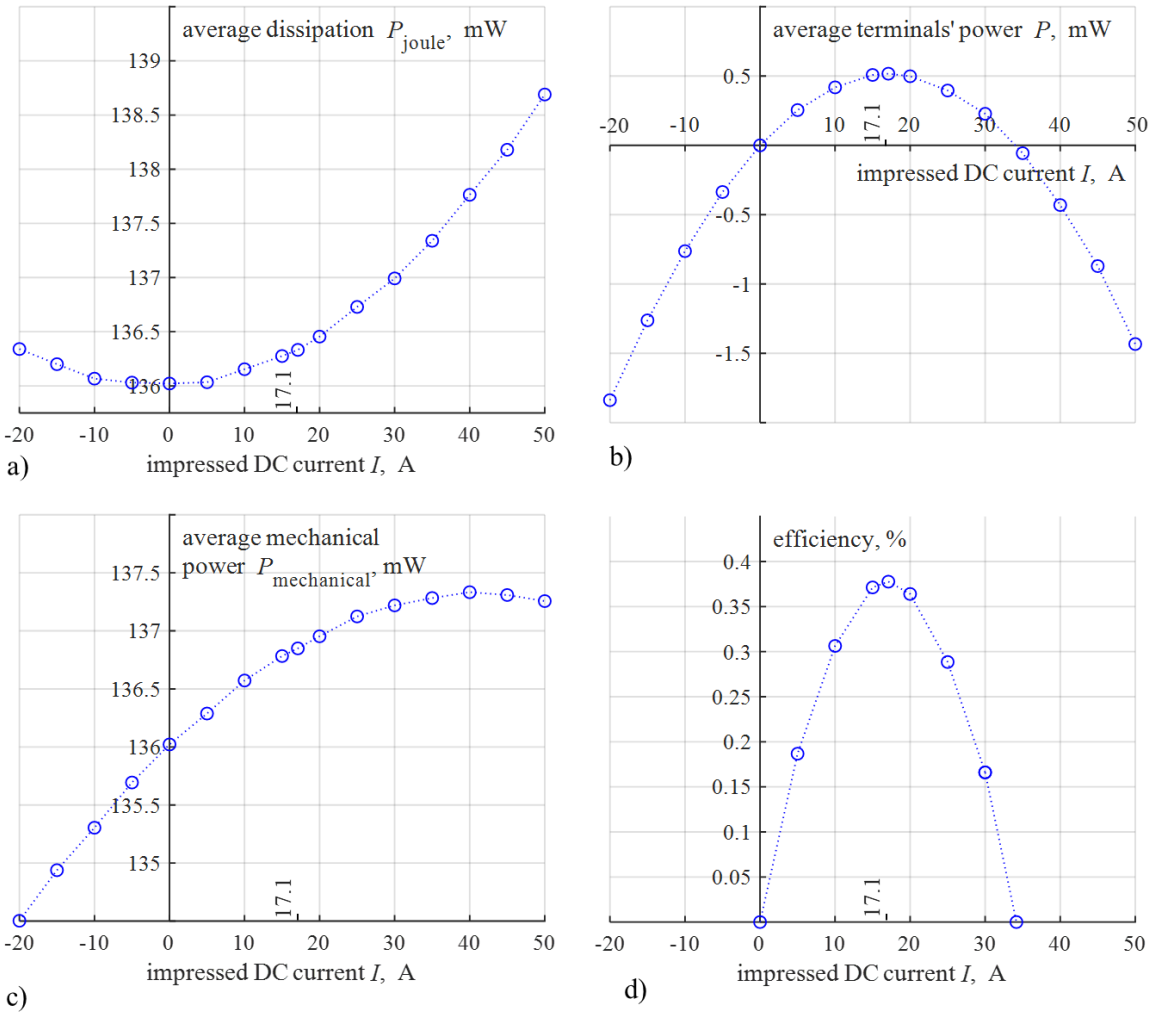

Figure 11. Average power per cycle and efficiency of the flux pump for different values of the DC impressed current.

IV.1.c Simplified equivalent circuit of the flux pump

The electromagnetic behavior of the flux pump is fully reproduced by means of the finite element based equivalent circuit of section *III*.a. However, the macroscopic behavior at the terminals can be reproduced by means of a simpler circuit obtained from empirical observation. This novel empirical equivalent circuit allows to investigate with good accuracy the interaction of the flux pump with an external component. For deducing this circuit, we first point out that both the instantaneous voltage V and the average voltage $V_{average}$ are, strictly speaking, affected by the total current I of the flux pump. To discuss the possible effects of this dependence, these two quantities are denoted with $V(t, I)$ and $V_{average}(I)$, respectively, in the following. It is observed in Figure 4 that, at any instant,

the higher the impressed current, the higher the deviation of the terminal voltage from the value obtained in no load conditions. Hence, the terminal voltage at any instant can be expressed as

$$V(t,I) = V(t,0) - R(t,I)\,I \tag{20}$$

where R is a parameter that depends, in general, both on t and I. By taking the time average of both sides of (20) in one period the following expression of the average voltage across the flux pump terminals is obtained

$$V_{\text{average}}(I) = V_0 - R_{\text{effective}}(I)\,I \tag{21}$$

in which V_0 is the average voltage in open circuit (no load) condition (V_0 = 58.9 μV - Figure 6) and $R_{\text{effective}}$ is a parameter referred to as effective resistance of the flux pump and defined as

$$R_{\text{effective}}(I) = \frac{\int_t^{t+T} V(t',0)\,dt' - \int_t^{t+T} V(t',I)\,dt'}{I} = \frac{V_0 - V_{average}(I)}{I} \tag{22}$$

From Figure 6 and Figure 7 a linear dependence of $V_{\text{average}}(I)$ is observed over a wide range of impressed currents. This trend is widely confirmed in experiments [4]-[8], and in the considered case applies for an operating current approximately within the interval from –100 A to +100 A (see Figure 7). Thus, within this linear interval, the following expression can be introduced for the average terminal voltage

$$V_{average}(I) = V_0 - \frac{V_0}{I_0} I \tag{23}$$

By substituting (23) in (22) we obtain

$$R_{\text{effective}} = \frac{V_0}{I_0}, \quad \text{independent on } I \tag{24}$$

An effective resistance $R_{\text{effective}} = 1.73\,\mu\Omega$ is obtained from the values of V_0 and I_0 for the considered flux pump, in agreement with [21]. Consistently with the results of Figure 6 and Figure 7 equation (24) states that the effective resistance is not dependent on the DC operating current of the flux pump, and is simply denoted with $R_{\text{effective}}$ in the following. We now assume that, provided that the current I is in the linear interval from –100 A to +100 A, the constant effective resistance $R_{\text{effective}}$ determines the difference between the instantaneous terminal voltage and the no load voltage. In other words, we assume that the time and current dependent resistance $R(t,I)$ in equation (20) can be replaced with the constant resistance $R_{\text{effective}}$ giving

(25) $$V(t,I) = V(t,0) - R_{\text{effective}}\, I$$

Based on equation (*25*) the empirical equivalent circuit of Figure 12.a, introduced in [4] and used in [6]-[8], [18],[21] for calculating the charging process of an RL load (not taking the ripple into account), is obtained. It is stressed that replacing $R(t,I)$ with a constant $R_{\text{effective}}$ is a merely heuristic assumption, whose validity is checked in the next section by comparing the results with those obtained with the finite element based equivalent circuit. It will be shown that, despite the equivalent circuit being deducted with reference to a DC operating current, it also applies when the current change with time, provided that the linear limit is not exceeded.

The equivalent circuit of Figure 12.a is widely used in the literature [4]-[8] [14]-[15] [18] [21] and allows to closely reproduce the dynamo's behavior in terms of terminals voltage and charging transient of the load. However, the existing equivalent circuitis not able to reproduce the dissipation that occurs in case of open circuit operation. This is an intrinsic dissipation, associated with the screening currents responsible of the rectification effect, that occurs independently on the load conditions and it is little affected by the operating current. In order to take this intrinsic dissipation into account the complete empirical equivalent circuit of Figure 12.a is introduced. In this novel circuit a resistor $R_{\text{intrinsic}}$ is added in parallel to the voltage source that is responsible for the intrinsic joule dissipation in no load condition. By denoting P_{joule0} with the average joule dissipation in one cycle occurring in no load conditions the value of $R_{\text{intrinsic}}$ is defined by

(26) $$P_{joule0} = \frac{\int_{t}^{t+T} \frac{V^2(t,0)}{R_{\text{intrinsic}}}\, dt'}{T}$$

which finally gives

(27) $$R_{\text{intrinsic}} = \frac{V_{\text{rms0}}^2}{P_{\text{joule0}}}$$

where V_{rms0} is the rms value of the open circuit voltage $V(t,0)$, that for the considered flux pump is 2.2 mV_{rms}. By considering the average dissipation of 135.9 mW in no load condition an intrinsic resistance $R_{\text{intrinsic}} = 34.2\,\mu\Omega$ is obtained for the flux pump. It must be noted that the Thevenin equivalent of the complete empirical equivalent circuit coincides with the partial one. Thus, with respect to the behavior at the terminals, the addiction of the resistor $R_{\text{intrinsic}}$ does not produce any effect. The same behavior is predicted for an external component connected to both circuits. During DC operation with impressed current I the average power in one cycle at the terminals follows the parabolic dependence given by $P_{\text{terminals}} = V_0 I - R_{\text{external}} I^2$ for both the circuits and is maximum at

$I = I_0 / 2$. The difference only exists in the average power delivered by the voltage source, that for the two circuits is given by

$$
\begin{aligned}
&P_{\text{source(partial)}} = V_0 I = VI + R_{\text{effective}} I^2 = P_{\text{terminals}} + R_{\text{effective}} I^2 \\
&P_{\text{source(complete)}} = V_0 I + \frac{V_{\text{rms0}}^2}{R_{\text{intrinsic}}} = VI + R_{\text{effective}} I^2 + \frac{V_{\text{rms0}}^2}{R_{\text{intrinsic}}} = P_{\text{terminals}} + \underbrace{R_{\text{effective}} I^2 + P_{\text{joule0}}}_{\text{overall joule dissipation}}
\end{aligned}
\tag{28}
$$

In the complete equivalent circuit, the voltage source delivers, besides the power at the terminal, the Joule power occurring in no load condition and an additional joule term corresponding to the dissipation on the effective resistance. A quadratic dependence of the overall joule dissipation on the current is obtained which is consistent with the parabolic trend shown in Figure 11.a, obtained with the FEM based model. The overall power delivered by the voltage source coincides with the mechanical power supplied to the rotor of the flux pump. The efficiency of the flux pump can be calculated as

$$
\eta_{\text{(complete)}} = \frac{P_{\text{terminals}}}{P_{\text{source(complete)}}} = \frac{P_{\text{terminals}}}{P_{\text{terminals}} + R_{\text{effective}} I^2 + P_{\text{joule0}}}
\tag{29}
$$

The average joule power, terminals' power and mechanical power in one cycle obtained with the complete equivalent circuit are shown in Figure 13a-c for different values of the DC impressed current and compared with FEM based data. The corresponding efficiency is shown in Figure 13d. The maximum difference between FEM data and complete circuit data is below 1.2 %. A good agreement exists, indicating that the partial equivalent circuit can replace the FEM based one with acceptable accuracy. An increasing mismatch is observed with increasing operating current, indicating that the circuit cannot be employed at high operating currents, outside the identified linear interval from –100 A to +100 A. No correspondence exists instead between the power of the voltage source, or the loss due to the effective resistance, of the partial equivalent circuit with the physical dissipation mechanisms occurring in the flux pump. No considerations on energy balance and efficiency can be done by means of this circuit.

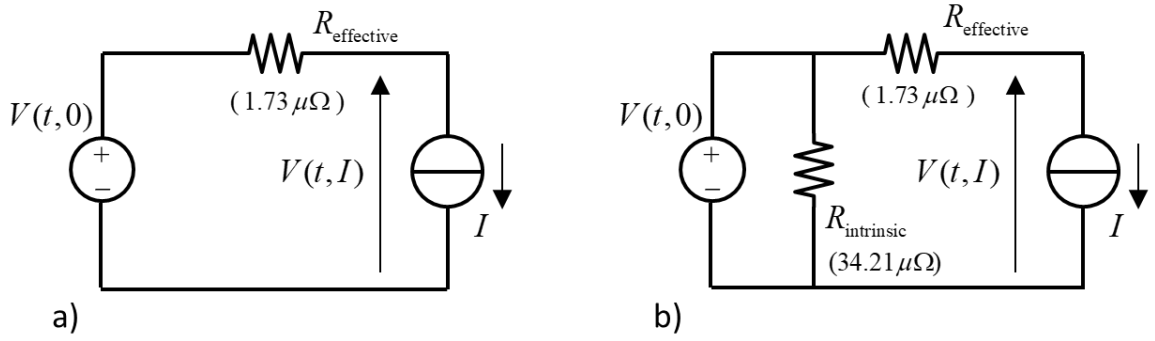

Figure 12. a) partial empirical equivalent circuit of the flux pump. b) complete empirical equivalent circuit of the flux pump taking internal dissipation into account.

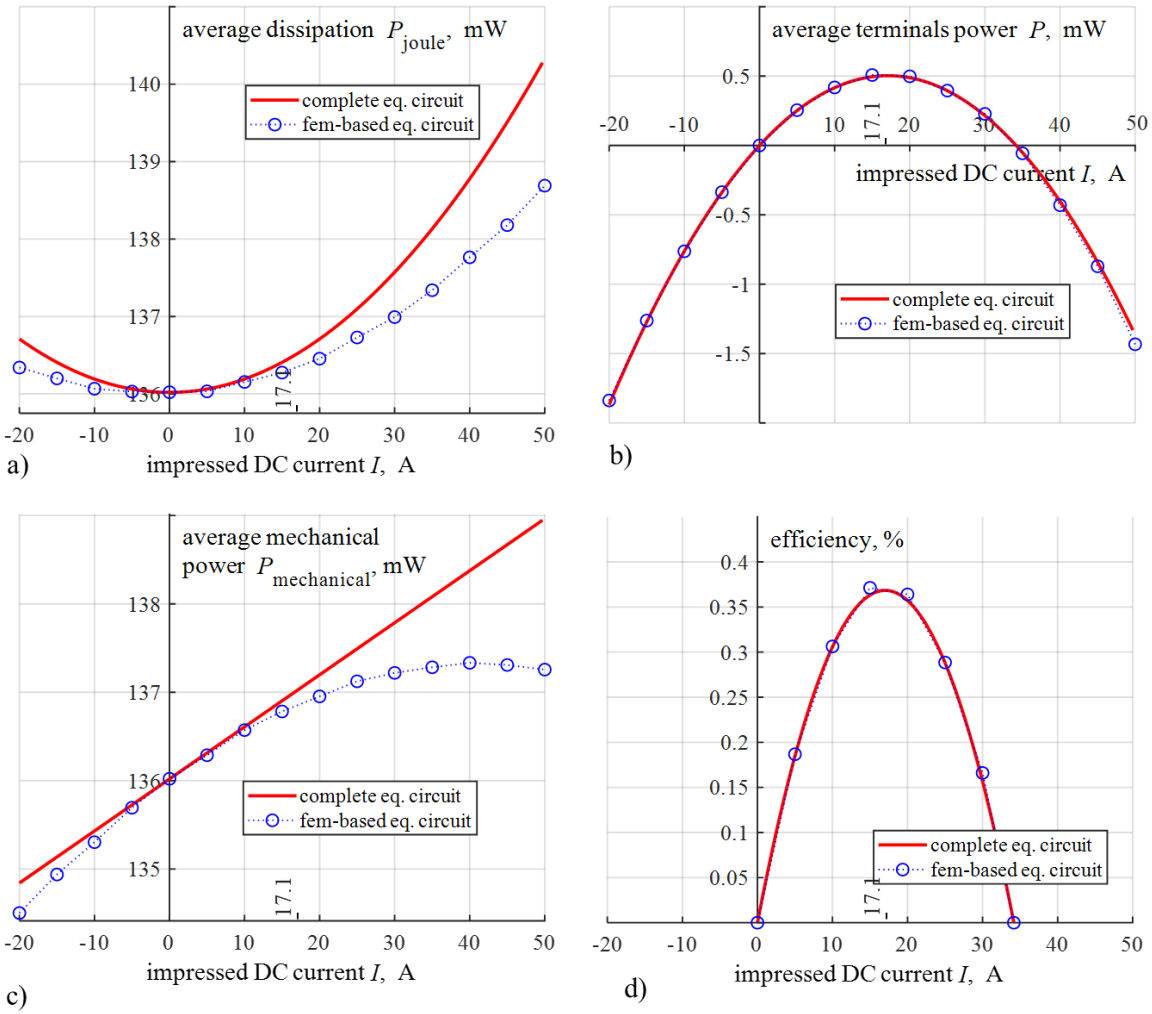

Figure 13. Average power per cycle and efficiency of the flux pump calculated by means of the complete equivalent circuit of Figure 12.b. FEM based data of Figure 11 are also replicated here for comparison.

IV.2 flux pump connected to an RL load

The numerical results referring to the flux pump supplying an RL load are discussed in this section. This operating condition can be used to model the charging of a HTS coil up to any current below the critical value. The short circuit operation of the flux pump can be seen as the limit case in which both the resistance and the inductance are set to zero.

IV.2.a Coil energization

As in [21], a coil with an inductance L_{ext} = 0.24 mH and resistance R_{ext} = 0.88 μΩ (due to joints) is considered in the following. The current of the *RL* load during 500 s is shown in Figure 14.b. Both the results obtained by means of the finite element model of section III and the by means of the complete equivalent circuit of section IV.1.c are shown. The latter are obtained by connecting the *RL* load to the complete equivalent circuit of the flux pump, as it is schematized in Figure 14.a. We do stress again that the current of the coil is not at all affected by the intrinsic resistor. In other terms, both including or not including $R_{intrinsic}$ in the circuit of in Figure 14.a, the same current in the coil is obtained. Including $R_{intrinsic}$ is only needed when a consistent energy balance of the flux pump needs to be assessed. The calculation of the steady state value and of the time domain evolution of the average value in one cycle of the current *I* of the coil by means of the equivalent circuit (with no intrinsic resistance considered) is a common practice in the literature [4], [6]-[8], [18], [21]. This is obtained by using a DC voltage source corresponding to the average value V_0 of the voltage $V_0(t,0)$ across the flux pump terminals in open circuit conditions. A final current $I_f = V_0 / (R_{effective} + R_{ext}) = 22.62$ A is injected into the coil by the flux pump, following the exponential charging law of the *RL* circuit with a time constant $\tau = L_{ext} / (R_{effective} + R_{ext}) = 92.16$ s. In this paper the equivalent circuit is used to capture the full time domain behavior to the coil's current, including the ripple. This is achieved by using a time changing voltage source which implements the full time evolution of the open circuit $V_0(t,0)$ voltage at any instant of one cycle, and replicating it in all simulating cycles. Figure 15 the detail of the current during 5 cycles after instant *t*=0 (corresponding to current *I*=0), and after instant t=150 s (corresponding to current *I*=18.18 A), is shown. No appreciable difference is observed between the FEM results and the results obtained with the equivalent circuit. This confirms that replacing *R*(*t*,*I*) with a constant $R_{effective}$ in equation (20) is indeed a viable approximation and the equivalent circuit, deduced with reference to a DC operating current, can be applied for time domain analysis, provided that the linear limit is not exceeded.

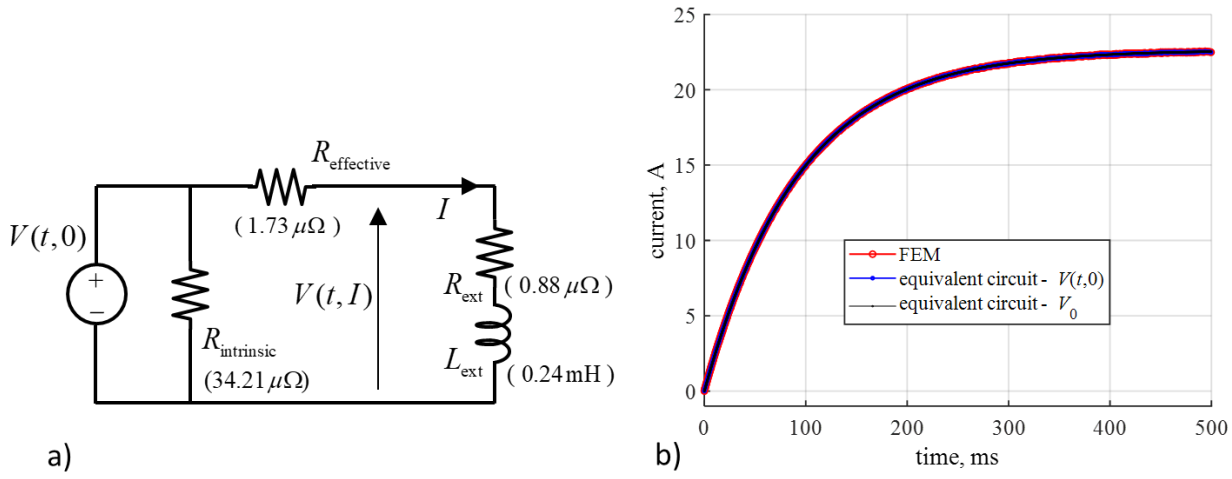

Figure 14. a) Complete equivalent circuit of the flux pump connected to a RL load b) Current of the RL load

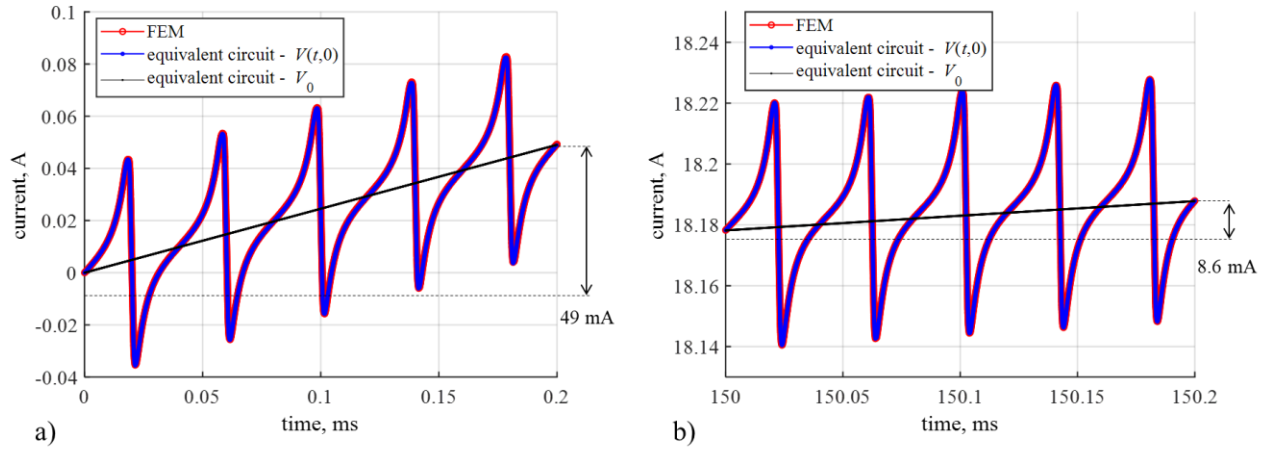

Figure 15. Detail of the current during 5 cycles after instant t=0 (when the current is null), and after instant t=150 s (when the current has reached reaches I = 18.18 A).

IV.2.b short circuit operation of the flux pump

In section IV.1.a it was shown that a null average voltage occurs at the terminals of the flux pump corresponding to DC impressed current I_0 = 34.2 A. Beyond this value, an average negative voltage appears on the flux pump that enters the dissipative mode. I_0 sets the limit of the generation ability of the flux pump and, despite the null voltage, should not be interpreted as the short circuit current of the flux pump, that is the current circulating in the flux pump when a short circuit connection is created at the terminals. The current circulating in this latter condition, calculated by means of the FEM based equivalent circuit by setting R_{ext} = 0 and L_{ext} = 0 in equation (*12*), is shown in Figure 16.a.

It can be observed that it changes periodically from –400 A to +400 A, resulting in a mean current of 225.9 A. In contrast, the current obtained by putting R_{ext} = 0 and L_{ext} = 0 in the equivalent circuit of Figure 14.a is shown in Figure 16.b. A completely different time behavior, with an average value of 34.2 A, is obtained in this case. This means that the short circuit of the flux pump creates operating conditions that are beyond the limit of applicability of the equivalent circuit. In particular, a peak current beyond 6 kA (absolute value) is reached in this case, which is inconsistent with the critical current of the wire that is 283 A. Using the fem model, a peak current of 400 A is reached, which is about 41 % above I_c. The highly resistive behavior of the tape developed according to the power law prevents the current to overcome this value. Hence, the equivalent circuit of the flux pump can only be used if the predicted current does not exceed, at any instant, this limit. This condition is usually satisfied when a current smoothing inductive load is considered.

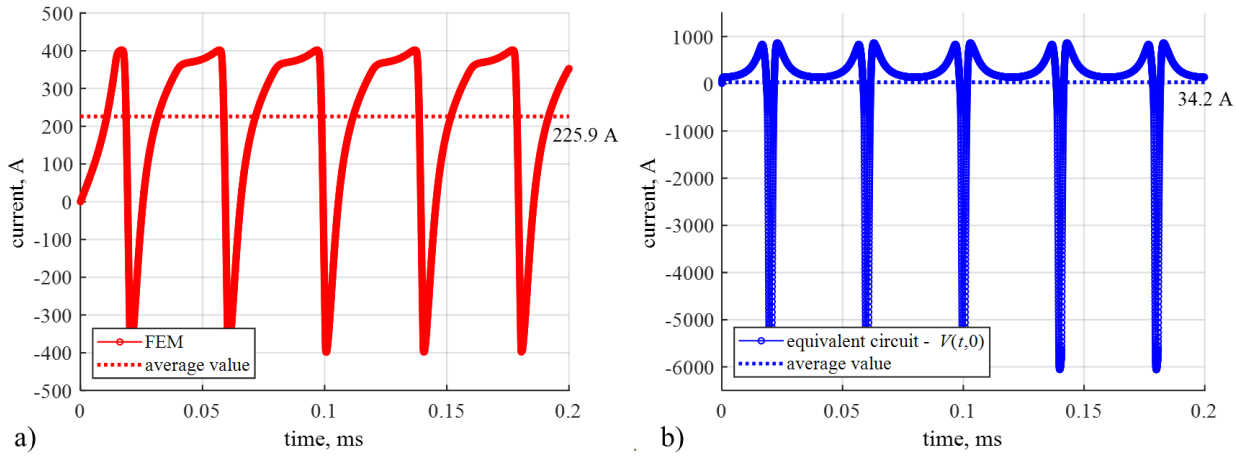

Figure 16. Total transport current flowing in the flux pump tape in case of short circuit operation. a) calculated by means of the fem model. b) calculated by means the equivalent circuit.

V. CONCLUSION

In this paper the energy behavior of the dynamo type flux pump was numerically investigated. It was shown that a resistant effect was produced, by the induced currents responsible for the DC voltage, against the rotor motion. Due to this interaction mechanism, a significant part of the mechanical power supplied to the rotor was found to be converted into Joule heating within the tape. The operational limits of the flux pump were also explored, showing that the generator mode, involving an electric power delivered to the load combined with a mechanical power supplied to the rotor, can only be achieved in a restricted range of current and voltage at the terminals and that the maximum power transfer and efficiency are reached at the middle of the generator range. In no

conditions the mechanical torque produced on the rotor can be reversed, reaching the motor mode involving an electric power absorbed at the terminals combined with a mechanical power produced on the rotor. A revised equivalent circuit, comprising besides the effective resistance commonly reported in the literature, a further intrinsic resistance was proposed, on an empirical base, for taking all the dissipation mechanisms into account. It was shown that this equivalent circuit is able to predict, with excellent agreement with finite element models, the energization of an RL load both concerning the charging transient and final steady value and the full time domain behavior of the current, including the ripples. All reported results were obtained by assuming a critical current of the tape independent of the magnetic field. Further investigation will be needed in the future for assessing the significant improvement of the power output, efficiency and operational limits of the flux pump that can be expected by taking the dependence of I_c on B into account.

References

[1] L. J. M. v. d. Klundert e H. H. J. ten Kate, «Fully superconducting rectifiers and flux pumps part 1: Realized methods for flux pumping,» Cryogenics, vol. 21, n. 4, pp. 195-206, 1981.

[2] L.J.M. van de Klundert and H.H.J. ten Kat, “On fully superconducting rectifiers and fluxpumps. A review. Part 2: Commutation modes, characteristics and switches”, Cryogenics, vol. 21, Issue 5, pp. 267-277, 1981.

[3] C. Hoffmann, D. Pooke e A. D. Caplin, «Flux Pump for HTS Magnets,» IEEE Transactions on Applied Superconductivity, vol. 21, n. 3, June 2011.

[4] Zhenan Jiang, K. Hamilton, Naoyuki Amemiya, R. A. Badcock, and C. W. Bumby , "Dynamic resistance of a high-Tc superconducting flux pump", Appl. Phys. Lett. 105, 112601 (2014).

[5] Jiang, Z., Bumby, C.W., Badcock, R.A., (...), Long, N.J., Amemiya, N., Impact of flux gap upon dynamic resistance of a rotating HTS flux pump, 2015, Superconductor Science and Technology, 28(11), 115008

[6] Jiang, Z., Bumby, C.W., Badcock, R.A., ...Sung, H.J., Park, M., A rotating flux pump employing a magnetic circuit and a stabilized coated conductor HTS stator Journal of Magnetics, 2016, 21(2), pp. 239–243.

[7] C. W. Bumby, A. E. Pantoja, H. Sung, Z. Jiang, R. Kulkarni and R. A. Badcock, "Through-Wall Excitation of a Magnet Coil by an External-Rotor HTS Flux Pump," in IEEE Transactions on Applied Superconductivity, vol. 26, no. 4, pp. 1-5, June 2016, Art no. 050.

[8] Chris W Bumby, Rodney A Badcock, Hae-Jin Sung, Kwang-Min Kim, Zhenan Jiang, Andres E Pantoja , Patrick Bernardo, Minwon Park and Robert G Buckley ,Development of a brushless HTS exciter for a 10 kW HTS synchronous generator.

[9] L. Fu, K. Matsuda, T. Lecrevisse, Y. Iwasa e T. Coombs, «A flux pumping method applied to the magnetization of YBCO superconducting coils: frequency, amplitude and waveform characteristics,» Superconductor Science and Technology, 2016.

[10] W. Wang, Y. Lei, S. Huang, P. Wang, Z. Huang e Q. Zhou, «Charging 2G HTS Double Pancake Coils With a Wireless Superconducting DC Power Supply for Persistent Current Operation,» IEEE Transactions on Applied Superconductivity, vol. 28, n. 3, April 2018.

[11] Y. Zhang, W. Wang, H. Ye, X. Wang, Y. Gao, Q. Zhou, X. Liu e Y. Lei, «Compact Linear-Motor Type Flux Pumps With Different Wavelengths for High-Temperature Superconducting Magnets,» IEEE Transactions on Applied Superconductivity, vol. 30, n. 4, June 2020.

[12] Geng, Jianzhao, et al. "Origin of dc voltage in type II superconducting flux pumps: field, field rate of change, and current density dependence of resistivity."Journal of Physics D: Applied Physics 49.11 (2016): 11LT01.

[13] T. A. Coombs, «Superconducting flux pumps,» Journal of Applied Physics, 2019.

[14] T. A. Coombs, J. Geng, L. Fu e K. Matsuda, «An Overview of Flux Pumps for HTS Coils,» IEEE Transactions on Applied Superconductivity, vol. 27, n. 4, June 2017.

[15] R. C. Mataira, M. D. Ainslie, R. A. Badcock e C. W. Bumby, Origin of the DC output voltage from a high-Tc superconducting dynamo, Applied Physics Letters, April 2019.

[16] M. Ainslie, F. Grilli, L. Quéval, E. Pardo, F. Perez-Mendez, R. Mataira, A. Morandi, A. Ghabeli, C. Bumby e R. Brambilla, «A new benchmark problem for electromagnetic modelling of superconductors: the high-Tc superconducting dynamo,» Superconductor Science and Technology, August 2020.

[17] A. Ghabeli e E. Pardo, «Modeling of airgap influence on DC voltage generation in a dynamo-type flux pump,» Superconductor Science and Technology, 2020.

[18] R. Mataira, M. D. Ainslie, R. Badcock e C. W. Bumby, «Modeling of stator versus magnet width effects in high-Tc superconducting dynamos,» IEEE Transactions on Applied Superconductivity, 2020.

[19] M. D. Ainslie, L. Quéval, R. C. Mataira e C. W. Bumby, Modelling the frequency dependence of the open-circuit voltage of a high-Tc superconducting dynamo, IEEE Transactions on Applied Superconductivity, 2021.

[20] Ghabeli, A., Pardo, E. & Kapolka, M. 3D modeling of a superconducting dynamo-type flux pump. Sci Rep 11, 10296 (2021). https://doi.org/10.1038/s41598-021-89596-4

[21] Asef Ghabeli, Mark Ainslie, Enric Pardo, Loïc Quéval and Ratu Mataira, Modeling the charging process of a coil by an HTS dynamo-type flux pump, Superconductor Science and Technology, Volume 34, Number 8

[22] Mataira, Ratu, et al. "Mechanism of the high-T c superconducting dynamo: models and experiment."Physical Review Applied14.2 (2020): 024012.

[23] J.Geng,B.Shen,C.Li,H.Zhang,K.Matsuda,J.Li,X.Zhang,T.Coombs “Voltage-ampere characteristics of YBCO coated conductor under inhomogeneous oscillating magnetic field” Appl. Phys. Lett.,108(26)(2016), Article262601

[24] Z. Jiang, C. W. Bumby, R. A. Badcock, N. J. Long, H. J. Sung, and M. Park, “A Rotating Flux Pump Employing a Magnetic Circuit and a Stabilized Coated Conductor HTS Stator,” Journal of Magnetics, vol. 21, no. 2. The Korean Magnetics Society, pp. 239–243, 30-Jun-2016

[25] John David Jackson, Classical Electrodynamics, 3rd Edition, Jhon Wiley & sons, August 1998, pp 208-212

[26] A. Morandi, M. Fabbri and P. L. Ribani, "Loops and Meshes Formulations for 3-D Eddy-Current Computation in Topologically Non-Trivial Domains With Volume Integral Equations," in IEEE Transactions on Magnetics, vol. 56, no. 10, pp. 1-14, Oct. 2020, Art no. 7401114, doi: 10.1109/TMAG.2020.3012632.

[27] A. Morandi, M. Fabbri, U. Melaccio, P. L. Ribani and G. Russo, “A volume integral equation based equivalent circuit for 3D calculation of the levitation force”, The 7th International Workshop on Numerical Modelling of HTS, Nancy-France (held on-line), June 23, 2021, On-line, available at https://htsmod2020.sciencesconf.org/315996

[28] A. Morandi, «2D electromagnetic modelling of superconductors, 2012, Superconductor Science and Technology, Volume 25, Number 10, 104003

[29] A. Morandi e M. Fabbri, «A unified approach to the power law and the critical state modeling of superconductors in 2D», 2015, Superconductor Science and Technology, Volume 28, Number 2, 024004

[30] Campbell A 2019 A circuit analysis of a flux pump *Supercond. Sci. Technol.* **32** 115009

[31] Zhang, M. Zhang, and W. Yuan, An efficient 3D finite element method model based on the T-A formulation for superconducting coated conductors", Superconductor Science and Technology, vol. 30, no. 2, p. 024 005, 2016. doi:10.1088/1361-6668/30/2/024005